

Study of Fatigue Endurance on Artificially Aged Additive Manufactured AlSi10Mg After Stress Relieved and Hot Isostatic Pressed + T6

L. A. Barrera, F. Medina, E. Arrieta. L. Marquez

**W. M. Keck Center for 3D Innovations, Department of Mechanical Engineering, The
University of Texas at El Paso, TX, 79968**

Abstract

Laser Powder Bed Fusion (LPBF) AlSi10Mg is used in the aerospace and automotive industries for its refined microstructure and ductility compared to cast alloys. However, LPBF processes can inherently lead to defects that may act as fatigue crack initiators, such as lack of fusion, balling, and keyhole porosity. This work focuses on the analysis of high-cycle fatigue (HCF) endurance of AlSi10Mg under expected service conditions. For this study, AlSi10Mg specimens were printed on an EOS M290 LPBF system and heat-treated by stress relief (SR1) and Hot Isostatic Pressing + T6 (HIP+T6), as per ASTM 3318. Specimens were subsequently artificially aged at 177°C for 0, 10, 100, and 1000 hours. HCF, as per ASTM E466, was conducted to determine the endurance of the specimens at various stress levels. Results revealed a stark difference in the fatigue life of the two stress levels, with SR1 results consistently high at the low stress level, exhibiting variances due to defects, HIP+T6 showed a steady decline as the aging parameter increased.

Introduction

In the world of additive manufacturing (AM), one of the most seen alloys used by Laser Powder Bed Fusion (LPBF) is AlSi10Mg, a versatile alloy employed because of its lightweight yet tough nature, its corrosive resistance, its thermal conductivity, and its good weldability due to its near eutectic Al and Si composition [1-3]. When printing AlSi10Mg by LPBF, it can have a density of ~2.66 g/cm³ and comes with a low melting point between 570°C and 590°C [2]. Printing AlSi10Mg with LPBF also offers the benefit of a refined microstructure due to the heating and cooling rates the parts experience during the in-process stage [3]. While the cooling rates yield greater mechanical properties, the high temperatures can cause residual stresses that may lead to premature failures in application [4]. More defects such as balling, lack of fusion, and geometric errors, all related to the machine's speed, power, layer thickness, and hatch spacing, can lead to porosity within the structure of the build. Porosity then leads to early fracture formation and a low and inconsistent service life [5]. With lack of fusion being identified as one of the leading fatigue life inhibitors [6].

To this end, the use of heat treatments has been implemented to mitigate these issues. Hot isostatic pressing (HIP) has seen a surge in use for treating as-built parts due to its ability to shrink pores, which are most commonly caused by entrapped gas that directly affects the material's mechanical properties [5] [7]. By utilizing HIP and its ability to reduce internal porosity, the material's fatigue life is subsequently extended [8]. Merino et al. [9] investigated the effects of multiple heat treatments on AlSi10Mg, including SR1, SR2, HIP, and HIP+T6 at various aging

times, compared to as-built. It was determined that there was a detrimental effect to the alloy after the aging processes within the heat treatment, given the Yield Strength (YS) and Ultimate Tensile Strength (UTS) for the 1000 hours aged as-built samples came out to be 231 ± 9 MPa (2.53% decrease), and 391 ± 5 MPa (15.56% decrease), respectively. For the HIP+T6, YS was 94 ± 4 MPa (60.83% decrease), and UTS at 144 ± 6 MPa (52.79% decrease), yet elongation was reported to see a significant increase from 4.6% for as-built, compared to the 28.9% for HIP+T6. At no aging hours, HIP+T6 still showed a larger percentage in elongation than the as-built specimen, with a difference of 8.6%. In a study conducted by Kumar Ramavajjala et al. [10] regarding heat treatment and print parameters on SLM AlSi10Mg. Kumar found that conventional heat treatments often increase ductility and fatigue performance through precipitates yet deteriorate the YS and UTS, along with reducing hardness values. As-built conditions exhibited higher YS and UTS, with low ductility and poor fatigue performance. It is suggested a more tailored treatment will improve material properties.

As studies continue, more specific approaches are being considered, as more particular parts are manufactured. For this purpose, this study focuses on the investigation of the effects of aging within HIP+T6 and SR1 heat-treated AlSi10Mg through high cycle fatigue (HCF) testing, simulating service temperatures through aging at 0, 10, 100, and 1000 hours. The samples were printed in the XY and Z orientations, resulting in 96 samples that were analyzed. The samples are categorized into their aging hours, print direction, and heat treatment, divided into four categories of aging hours, with 24 samples each, further divided into their orientation, splitting the samples into 12 for XY and Z respectively, and divided into two batches, the SR1 and HIP+T6 treated, giving out 6 samples for each group.

Materials and Methods

The powder used was gas-atomized AlSi10Mg Valimet's AM 103 C grade. With this powder, all 96 specimens were created. Characterization was conducted using a Retsch Camsizer X2 (Haan, Germany). The powder had a size distribution with d10: 25.2 μ m, d50: 38.6 μ m, and d90: 59.2 μ m, displayed in Figure 1, values which correspond to the coarse level powder as specified by the C grade[11]. The powder exhibited an alpha-Al dendritic composition, as illustrated in Figure 2, with most particles being spherical and a few elliptical.

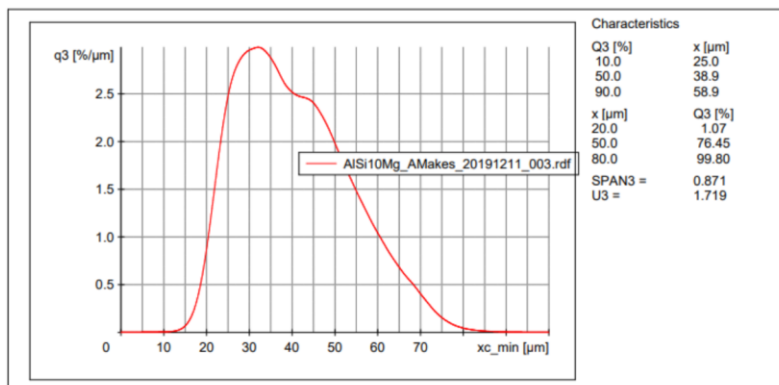


Figure 1: Valiment's Powder Distribution

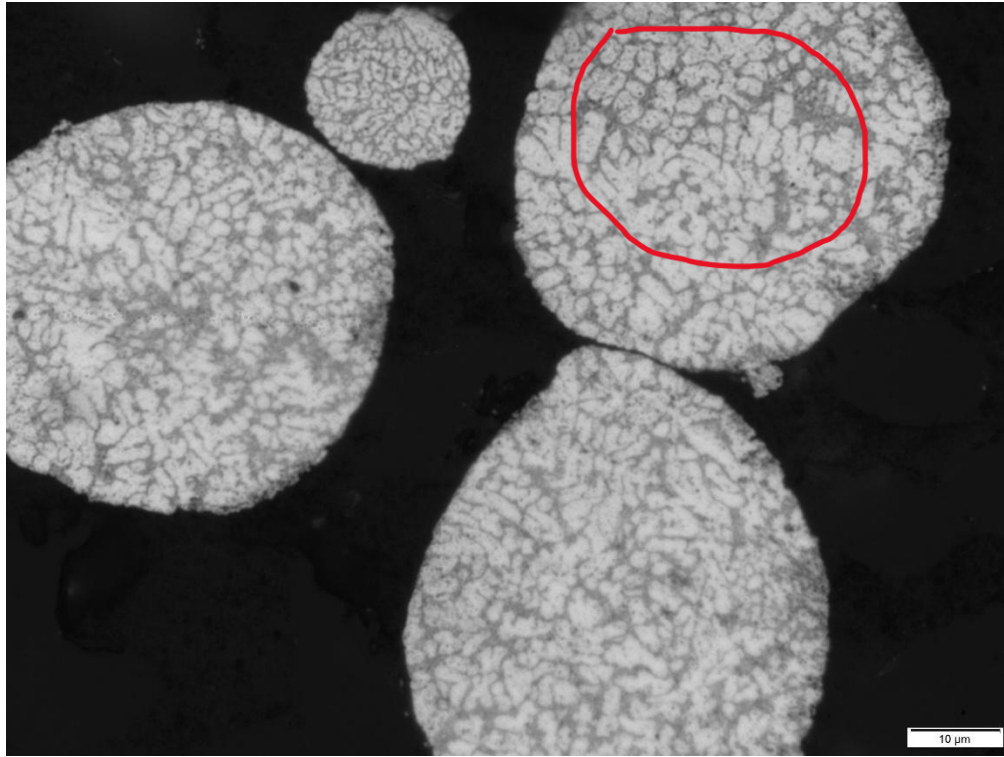


Figure 2: Powder Microstructure (alpha-Al dendritic composition circled in red)

The printing system utilized was an EOS M290 L-PBF system. The machine offers a build volume of 250 x 250 x 325 mm, featuring a 400 W, Yb-fiber laser and a scanning speed capable of reaching up to 7.0 m/s [14]. The print parameters used on the EOS M290 for this experiment's coupons are displayed on Table 1. These parameters contributed to achieving an average density of 2.65g/cm³, as measured by HE pycnometry. With an apparent density of 99% for all samples across all aging, heat treatments, and print orientation, analyzed through the microstructure. Coupons were machined down in accordance with the E466 standard.

Table 1: EOS M290 Print Parameters

Laser Power	Scanning Speed	Hatch Distance	Layer Thickness	Preheat Bedplate Temp.
300 W	1000 mm/s	130µm	30µm	80°C

The heat treatment of SR1 and HIP+T6 was conducted with the F3318 standard. SR1 heat treatment was held at 285°C for 120 min, and subsequently cooled at an air cooling rate. HIP+T6 was conducted at two different stages (HIP and T6); HIP was conducted under an inert atmosphere

with an applied stress of 100 MPa, within 510°C, kept at a selected temperature within plus or minus 25°C for 180 minutes, and cooled within the same inert atmosphere to below 93°C. T6 follows HIP with a temperature held at 530°C for 360 minutes, followed by quenching in water and artificially aged at 160°C for 360 minutes again. It is prudent to note that the aging process that occurs within T6 is not added onto the aging parameters that will be studied in this research, it is its own parameter that is taken as a step in the whole of T6, not the studied aging process.

Samples were CT-scanned through a PIXS CT (Duluth, Georgia) by Pinnacle X-RAY Solutions. This was done in order to acquire porosity and inclusion counts, while also seeing the progressive effects the aging and the heat treatments had within the sample pieces.

Printed samples were subsequently sectioned and analyzed for microstructure characterization. Samples were hot mounted with the ATM OPAL 460 (Haan, Germany) using epoxy. They were then grinded and polished by an ATM SAPHIR 530. Samples were ground with 320 grit paper, twice, at 1 minute per paper, 25N, with a rotating speed of 240 rpm. Grinding was followed by polishing with a diamond disc using a 9 µm suspension for 3:30 minutes at 25N and 150rpm. Then, white wool cloth disc with 3 µm suspension, 3:30 minutes, 20N, and 150rpm. The final polishing step of .2µm suspension at 3:30 minutes, the last 30 seconds, samples were polished over water, no suspension; the process used 10N and 150rpm. The microstructure was revealed using Keller's reagent.

Hardness testing was performed using Struers Duramin-A300 (Struers, Cleveland, OH, USA). Measurements using Vickers scale (HV) were attained from each sample, on the Y-Z plane for XY built direction, and from the top section on Z samples. Load of 100gf with 5s dwell time. 6 indentations were performed, three parallel to three.

The fatigue testing was conducted under the force-controlled standard of ASTM-E466 by an external laboratory. Testing was performed at room temperature (20-24°C) by servo-hydraulic test equipment, employing a sinusoidal waveform at a test frequency of 50Hz and R-ratio of 0.1. Run-out tests were considered as any sample that withstood over 5,000,000 cycles. The axial HCF stress levels varied for each heat treatment; SR1 saw 124 and 193 MPa stress levels, while the HIP+T6 saw 145, 193, and 269 MPa stress levels. The stress levels were determined by the YS and UTS originally obtained from past research [7]. YS and UTS coming out to be 157 and 247 MPa, respectively, for SR1. HIP+T6 saw a YS and UTS of 201 and 269 MPa, respectively. These values were used to represent the stress levels; on HIP+T6, the 193 MPa stress level was meant to represent the material at its YS, while the 269 MPa was intended to be close to its UTS. Yet these numbers were skewed due to early testing showing that HIP+T6 had a short cycle life when tested at 269 MPa, so the stress level was reduced to 145 MPa for the remaining testing sequence.

Results and Discussion

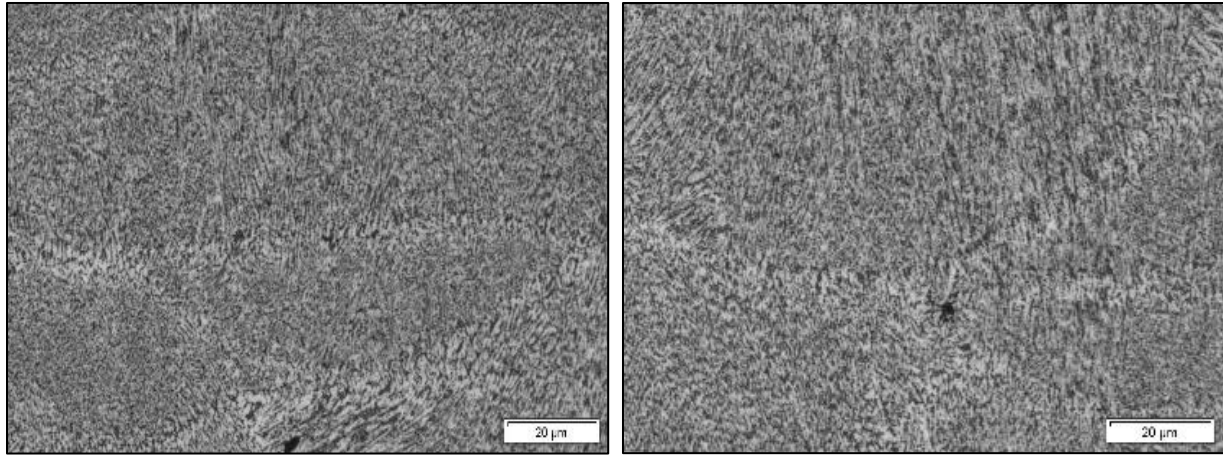
The hardness test conducted showed the relation between the hardness of the alloy and the aging hours. The build direction also had an effect on samples; however the major difference is

evident between the two heat treatments, HIP+T6 and SR1, as portrayed on Table 2. The density of the samples came out to be 2.65g/ cm³, for SR1 and 2.65g/ cm³ for HIP+T6 and did not see a change through the aging parameters; the only difference between the apparent density percentage was SR1, with a lower average density ranging between the aging hours from 99.13 to 99.07%, compared to HIP+T6 with 99.34-99.19% (density percentage was taken from sectioned samples faces, different cut samples could show different percentages). Hardness levels saw a decline as aging parameters increased on the side of HIP+T6 samples, seeing a change from 0 aging hours with an HV of 106 in the XY direction and a higher value of 121 HV in the Z direction at 0 aging hours to 59 HV at 1000 hours on XY direction, and 58 HV on Z direction, indicating a direct effect from the aging hours to the hardness of the alloy. SR1 saw a dissimilar interaction between its HV and the aging parameters. Specifically in the Z direction, the aging boosted the HV value from an original 89 HV at 0 aging hours to 105 HV at 100 aging hours, with a decline below the 0 aging hours at 1000 hours. HV on the XY direction from SR1 showed steady figures throughout the aging up to 100 hours, but just as the Z direction samples, the XY sample exhibited a decline at 1000 hours.

Table 2: Hardness Values of Samples

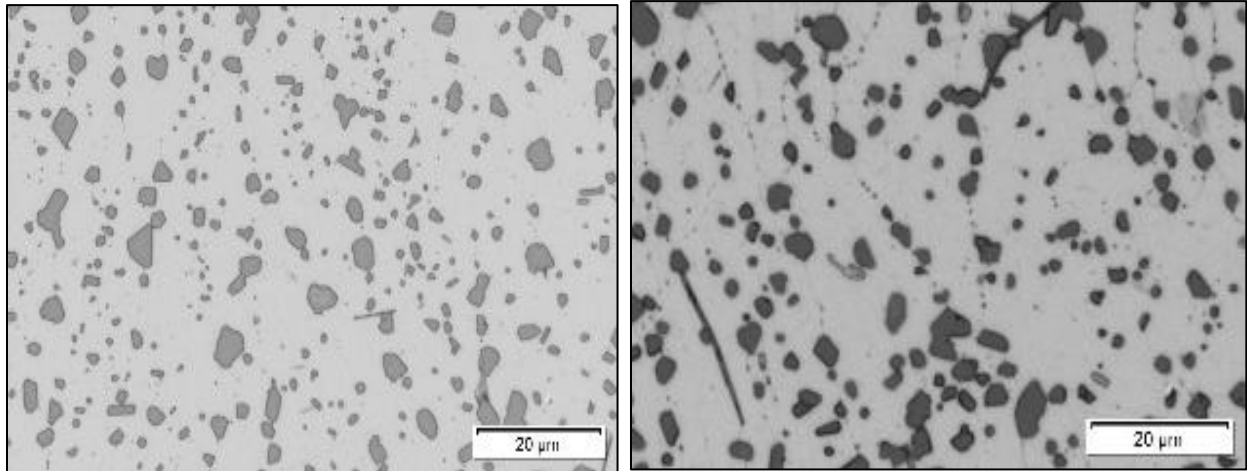
Test Matrix for SR1 and HIP+T6	XY-Build Direction		Z-Build Direction	
	Aging (hours)	Hardness (HV)	Aging (hours)	Hardness (HV)
SR1	0	93	0	89
	10	95	10	98
	100	94	100	105
	1000	86	1000	84
HIP+T6	0	106	0	121
	10	110	10	110
	100	73	100	81
	1000	59	1000	58

The microstructure pictures shown in Figures 3 and 4 (a-d) represent the samples at 0 aging hours for HIP+T6 and SR1 in the XY and Z directions. SR1, viewed along the XY and Z directions, displays a fine cellular near-eutectic structure from the aluminum and silicone mixture, where the melt-pool tracks are visible. The microstructure is comprised of ultra-fine cell structures that show a slight variation between the orientations. HIP+T6 microstructure is quite different, showing a distribution of size-varying coarse Si precipitates that are thermally stable through the Al composition, with slashes categorized as AlFeSi; these precipitates affect the strength of the alloy and, in large quantities, can lower the mechanical properties. The microstructure shape of the HIP+T6 samples is a direct result of the HIP heat treatment since the microstructure becomes homogenous and the melt-pools are eradicated [12].



(a)

(b)



(c)

(d)

Figure 3: Microstructure of 0 hours XY and Z planes (SR1, (a) XY direction, (b) Z direction and HIP+T6, XY (c), and Z (d))

The microstructures for the XY and Z orientations of SR1 and HIP+T6 after 1000 hours of aging are displayed in Figure 4 for comparison. No significant changes were observed except for the mechanical properties which will be discussed in the fractography section.

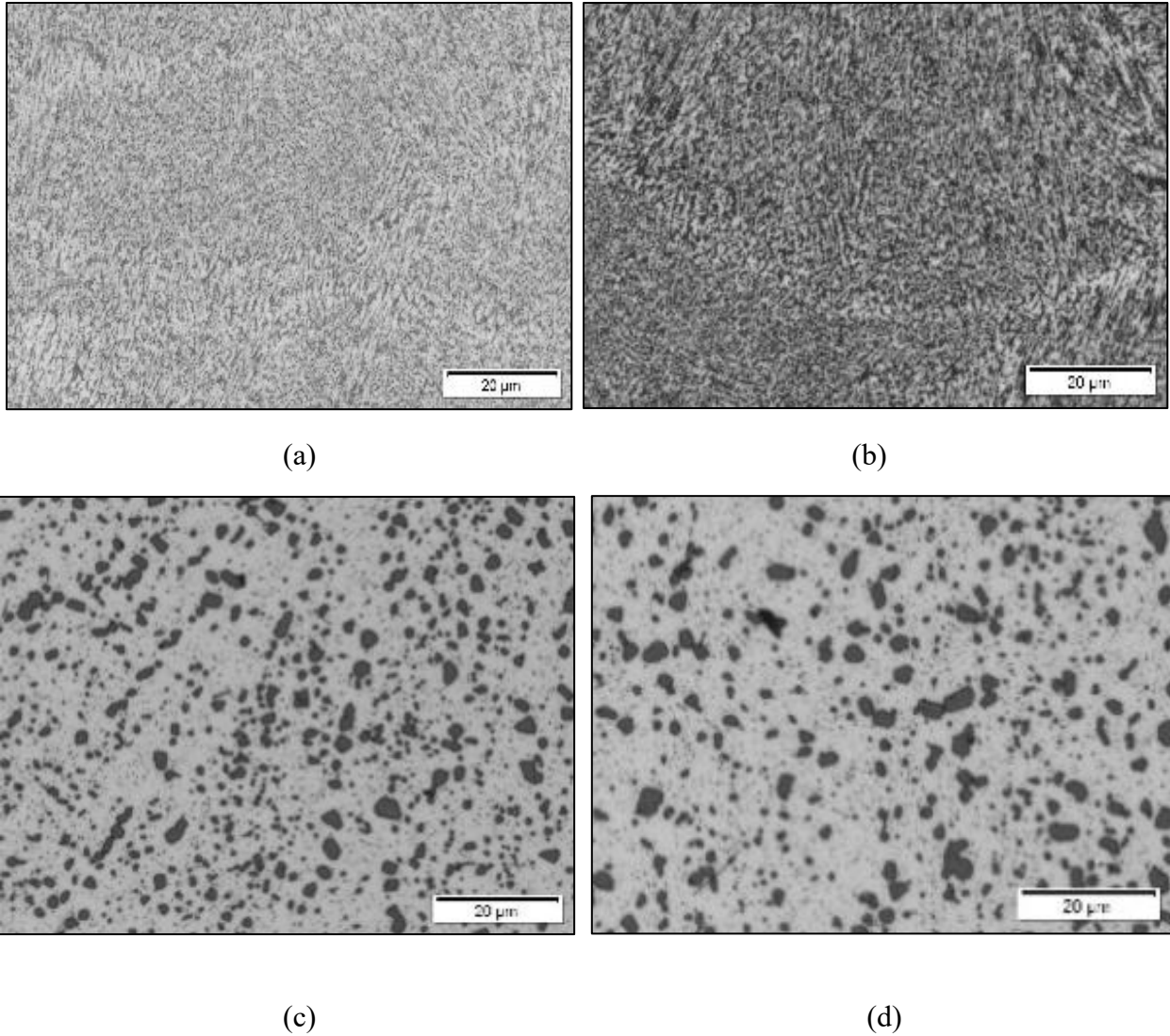


Figure 4: Microstructure of 1000 hours XY and Z planes (SR1, (a) XY direction, (b) Z direction and HIP+T6, XY (c), and Z (d))

The fatigue testing was conducted on all 96 samples, including both the elastic and plastic region for SR1, and on samples with HIP+T6 at 145, 193, and one 269 MPa. The results for both samples are portrayed in Table 3 and Table 4, respectively. Some changes were applied to the stress levels on HIP+T6 samples, given their weak resistance to the initial test of 269 MPa (263 cycles at 0 aging). The original test level of 269 MPa was reduced to 145 MPa, and with further testing, specifically at 1000 hours, the samples from 193 MPa were adjusted to 145 MPa due to their weak nature. The reduced number of samples within the 0 aging hours on XY and Z direction on HIP+T6 was because of an original sample being tested at 269 MPa, which was discarded for the new 145 MPa metric, and the Z sample was moved to the 193 MPa stress level for further testing since the 145 MPa would have resulted on another run-off specimen.

For the most part, the SR1 samples tested at 124 MPa were run-offs, yet some oddities occurred within the testing, seeing them start from 10 hours of aging. Since these results were not consistent, this can be related to residual porosity found within the microstructure, resulting in sporadic failure. SEM imaging revealed that most defects originated from lack of fusion, becoming points of crack initiation, as shown in Figure 5. The 1000-hours aging XY sample with 4,535,235 cycles was considered a failure due to fracturing at the grip, rather than the desired gauge section, the value can be discarded. The trajectory of the cycles can be analyzed on the S-N curves provided in Figures 6 and 7.

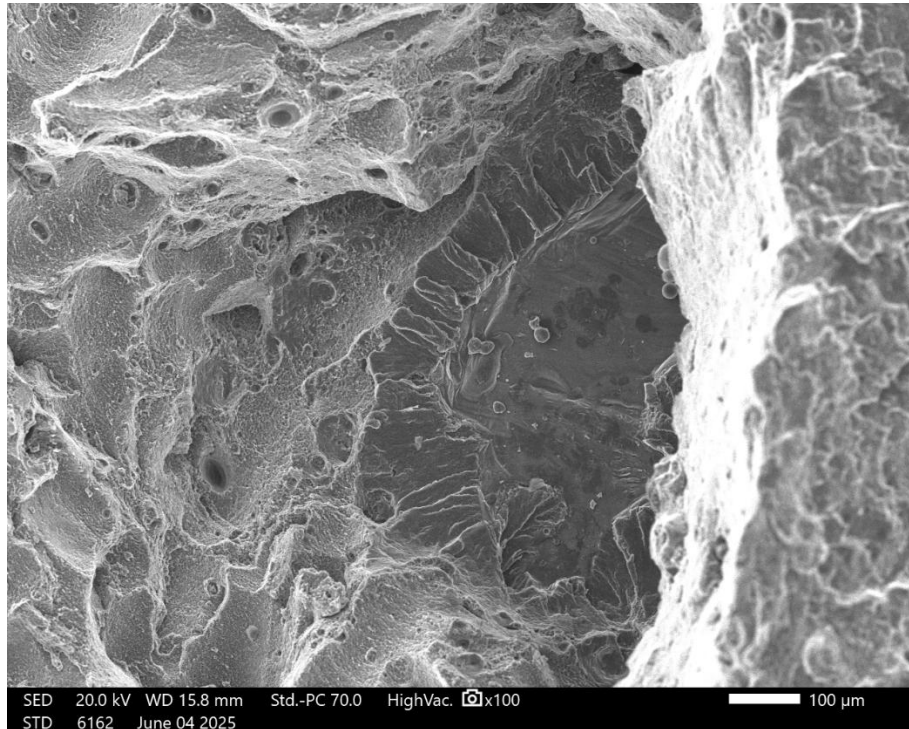


Figure 5: SEM image of Lack of Fusion

Through CT-scan, the porosity/inclusion amounts were able to be calculated. With this information, the behavior of the specimens could be predicted. The major point of interest regarded SR1 samples at 124 MPa, due to the sporadic failures that occurred through the testing, as mentioned previously. Looking at Table 3, the failure that occurred at 10 hours of aging (917,687), compared to one of the run-offs in the same category, were analyzed to contrast the CT-scan results. The failure sample had an overall count of 2,678 pores/inclusions, while the run-off sample counted 2,105 pores/inclusions, a difference of this magnitude relates to the early failure. For a more staggering comparison of the difference between the samples from SR1 at 124 MPa, aged for 100hrs, the three samples see quite the difference in cycles withstood, through the CT-analysis conducted, the number of pores and inclusions were determined, the run-off sample was found to have 732 pores/inclusions, while the failure at a million cycles was found to have 2,527 pores/inclusions within its mass. With the differing number of pores and inclusions, the sample

were affected drastically differently, while being treated within the same heat treatment and at the same stress level, speaking to the effect these number of pores and inclusions can have within the fatigue performance.

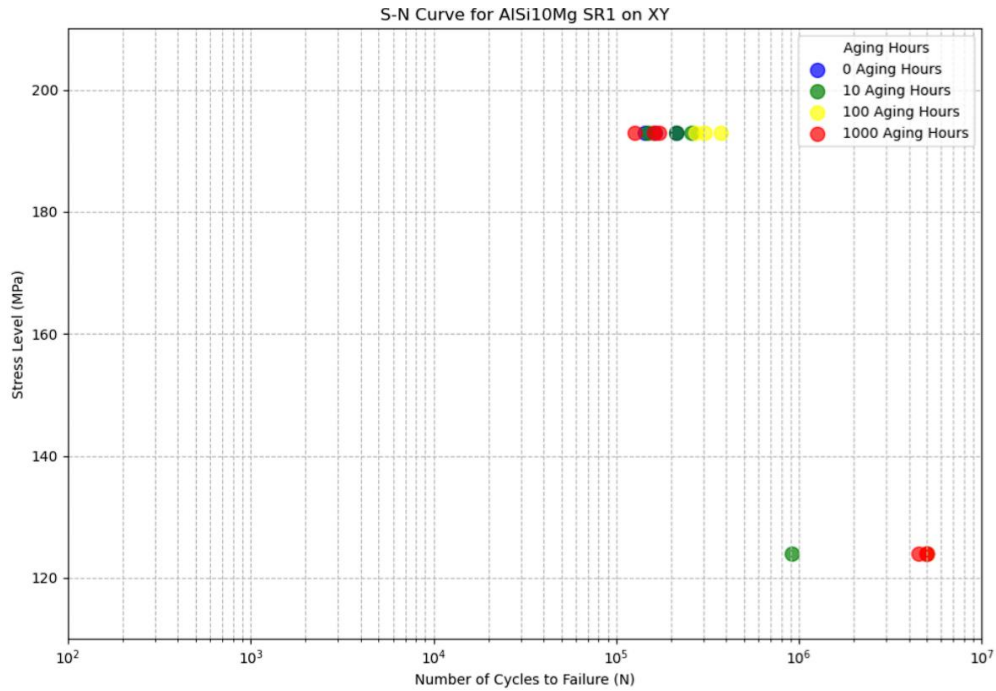
Table 3: Number of Cycles Matrix for SR1

HCF of AlSi10Mg SR1 Samples		Thermally aged at 177 °C							
		0 hours		10 hours		100 hours		1000 hours	
		XY	Z	XY	Z	XY	Z	XY	Z
STRESS LEVEL	124 MPa	5,000,000	5,000,000	5,000,000	5,000,000	5,000,000	592,677	4,535,235	5,000,000
		5,000,000	5,000,000	917,687	5,000,000	5,000,000	5,000,000	5,000,000	5,000,000
		5,000,000	5,000,000	5,000,000	5,000,000	5,000,000	1,208,462	5,000,000	5,000,000
	Average	5,000,000	5,000,000	3,639,229	5,000,000	5,000,000	2,267,046	5,000,000	5,000,000
STRESS LEVEL	193 MPa	211,910	145,313	148,899	46,019	371,566	277,879	160,278	152,880
		142,958	140,790	213,313	36,228	304,360	107,320	126,079	90,868
		163,846	214,049	258,026	94,838	271,262	80,786	172,349	75,217
	Average	172,905	166,717	206,746	59,028	315,729	155,328	152,902	106,322

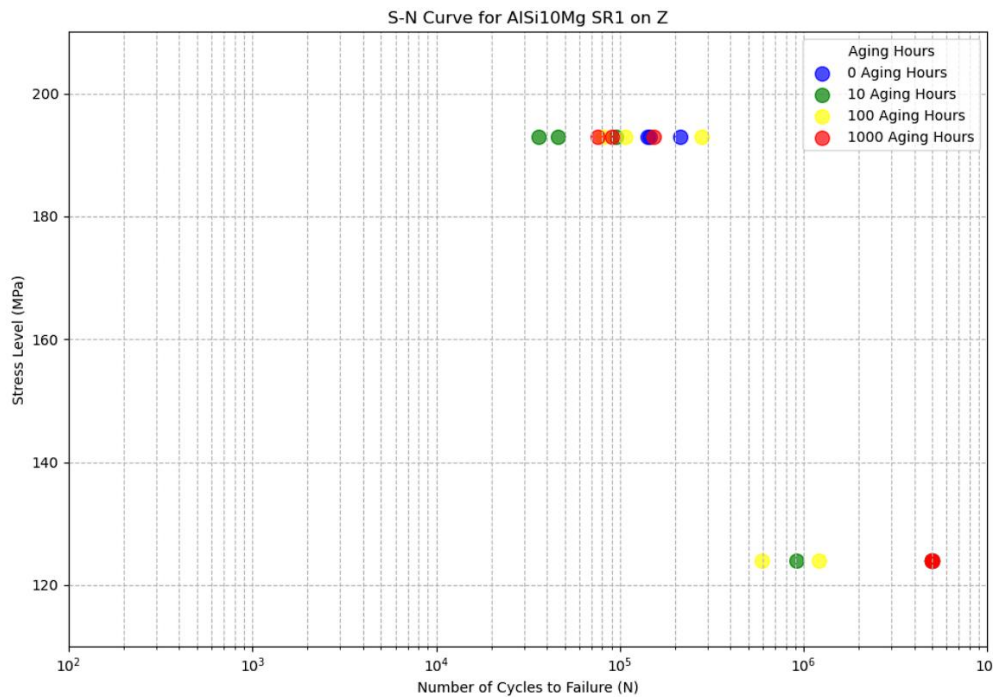
Table 4: Number of Cycles Matrix for HIP+T6

HCF of AlSi10Mg HIP+T6 Samples		Thermally aged at 177 °C							
		0 hours		10 hours		100 hours		1000 hours	
		XY	Z	XY	Z	XY	Z	XY	Z
STRESS LEVEL	145 MPa	5000000	5000000	5000000	5000000	5000000	5000000	197915	239189
		5000000	5000000	5000000	5000000	5000000	5000000	246314	1737
				5000000	5000000	5000000	5000000	104626	3896
									1579
	Average	5000000	5000000	5000000	5000000	5000000	5000000	182952	61364
STRESS LEVEL	193 MPa	1802403	5000000	3200960	404946	245898	91258	655	269
		256587	5000000	239263	107616	187778	231483	593	
		212245	470234	91944	5000000	131612	259210	646	
	Average	757078	2694734	1177389	1837521	188429	193984	631	269

The SR1 results at 193 MPa showed drastically different numbers of cycles, with none of them reaching 5,000,000 cycles anymore, and none even passing the 1 million mark. The Z direction exhibited an interesting interaction between its hardness levels and the cycles it endured, which could be explained by the coarsening of the Si particles within the structure [13]. However, the correlation to the cycles endured needs further investigation to have a more concrete solution; in contrast, the cycles in the XY direction saw an increase within the cycles up to 100 hours and a sharp decline on 1000 hours, which was as expected.



(a)

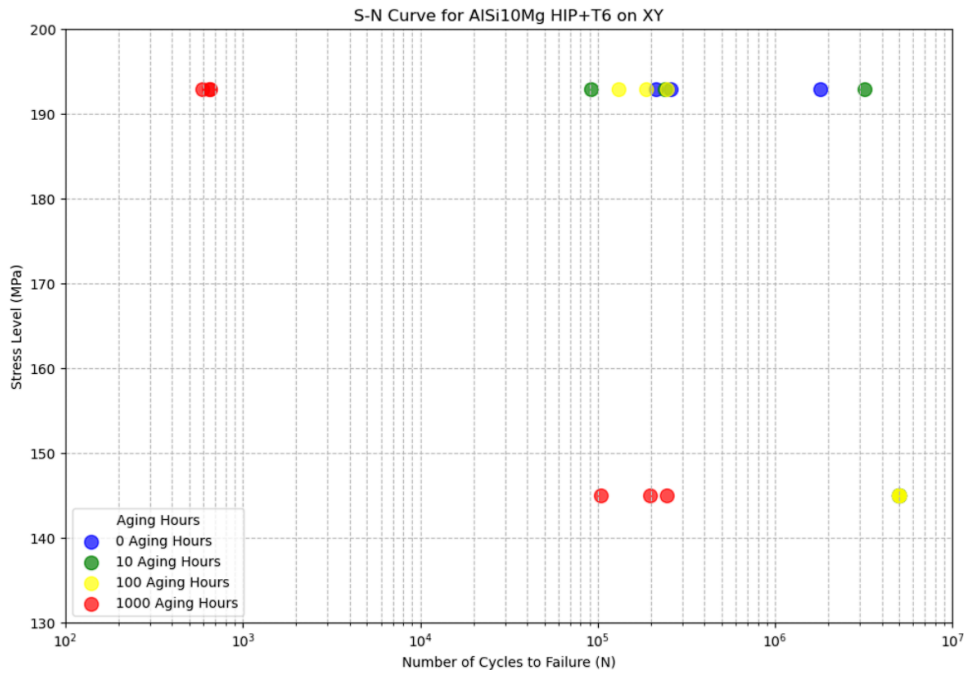


(b)

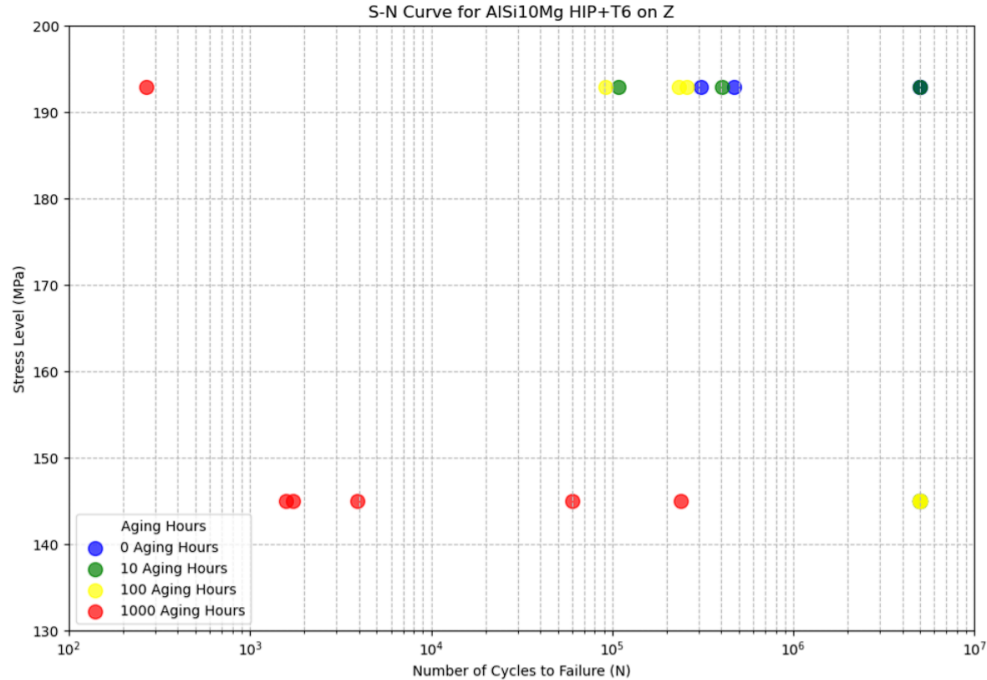
Figure 6: S-N curves for SR1 at (a) XY direction, and (b) Z direction

HIP+T6 yielded dissimilar results from the fatigue testing, with all 145 MPa tests up to 100 aging hours reaching the run-off state of 5,000,000, yet a sharp decline at 1000 hours, as per

SR1. For the 193 MPa stress level, some run-offs were experienced in the Z direction at 0 hours, which stands as an oddity due to the same testing samples at the same aging hours. The testing results showed a limited number of coupons and cycles survived. The built plate placement can be assessed to point out the variance in results, where the recoater can push finer powder particles in a single direction while other particles fill out the rest. Another element of the matrix to note, as stated previously, is the lack of test samples at 1000 hours and 193MPa. This was due to early testing resulting in a low number of cycles that did not reach the desired stress level. These samples were subsequently moved to the 145 MPa stress level, to obtain more accurate testing results.



(a)



(b)

Figure 7: S-N curves for HIP+T6 at (a) XY direction, and (b) Z direction

Fractography revealed the crack propagation and behavior of the specimens during fatigue testing. The SR1 images shown in Figure 8 exhibited clear fracture initiation points along the surface; all analyzed fractures proved to have originated from surface defects. The elastic fracture, compared to the HIP+T6 samples, exhibited a larger area of fracture propagation compared to the brittle fracture area, which explains the higher resistance to fatigue cycles. Upon examination, the surfaces exhibited a large amount of porosity, and points of lack of fusion. These are considered print parameters errors that can be mitigated and assessed through scan strategies to achieve far better results. A deeper analysis of the crack propagation was undertaken, by measuring the areas of the crack propagation and considering the defects sizes. The analysis was based on the 193 MPa SR1 samples, at its different aging parameters. This analysis revealed a varying size of crack propagation, with the first sample (0hrs) coming with an area of 7.34 mm², this sample saw the highest cycles in the analysis. The second sample (10hrs) saw a reduction in cycles, yet after analysis, it was found to have an area of 4.49 mm², this was due to the high number of larger defects, the crack initiation was started at a defect of 300µm, compared to the first sample which had a crack initiation defect of 100µm. The third sample analyzed (100hrs) sat at 11.32 mm², yet didn't see the highest amount of cycles, this can be explained by the size of the crack initiation defect of 170µm, multiple defects were also found across its surface in higher quantities than the first sample. The final sample (1000hrs) came out with a propagation area of 9.47 mm², with a higher number of cycles than that of the third

sample analyzed. It had a smaller crack initiation defect of 150 μ m compared to the third sample, yet still higher than that of the first sample.

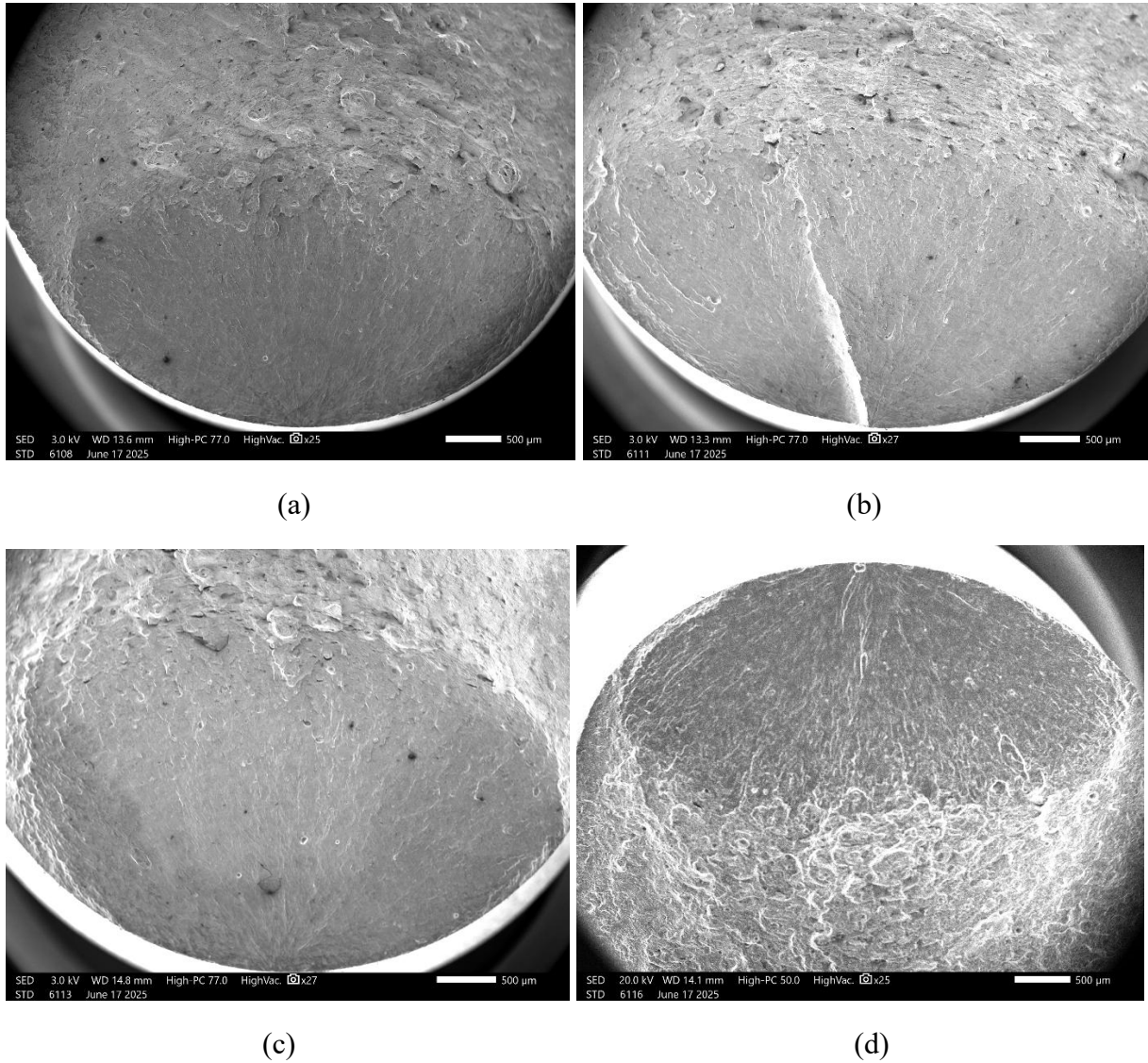
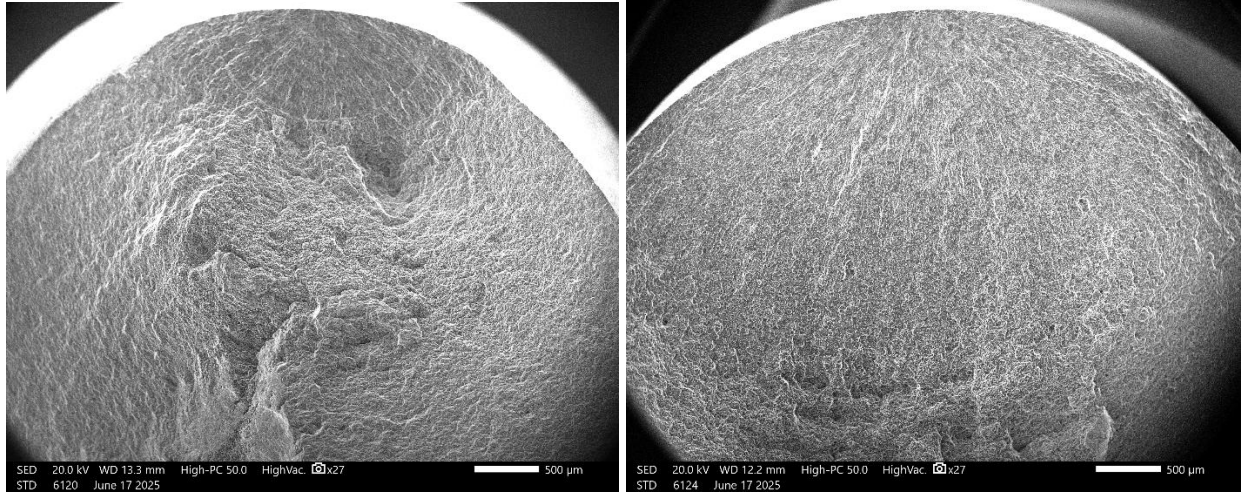


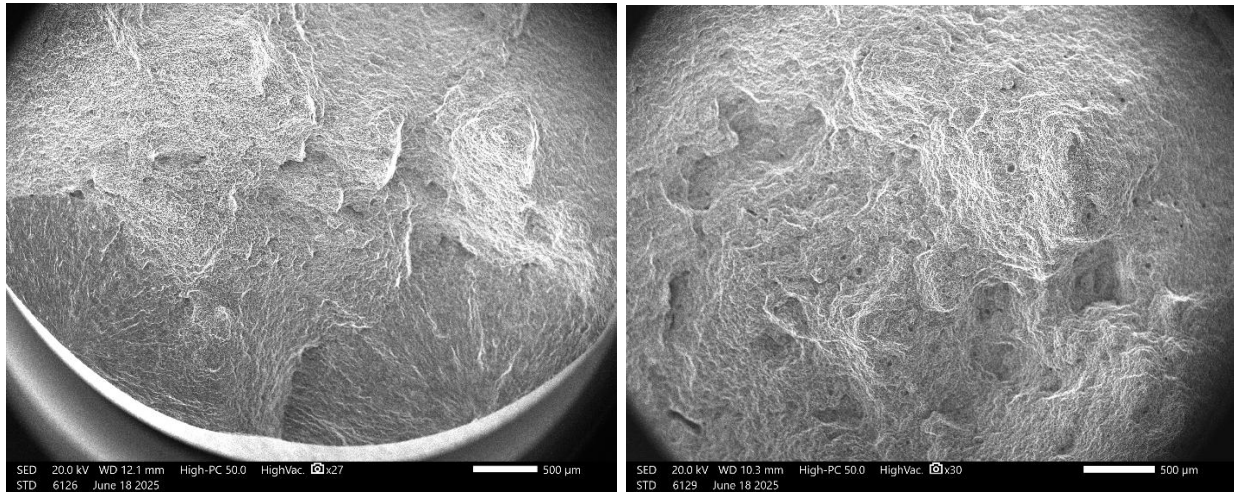
Figure 8: SR1 fractography images (0 (a), 10 (b), 100 (c), and 1000 (d) hours)

The fracture propagation area of the HIP+T6 samples, as stated earlier, was smaller, represented in Figure 9. However, at 10 aging hours, the sample's fracture path seemed comparable in size to those from SR1. The 1000 aging hours also saw a reduction in diameter, caused by the ductility gained from the high temperature. Another notable representation of the gained ductility is the lack of a fracture initiation point on the 1000 hours, giving it elongated through the cycles survived.



(a)

(b)



(c)

(d)

Figure 9: HIP+T6 fractography images (0 (a), 10 (b), 100 (c), and 1000 (d) hours)

A significant indication of ductility within a sample is the presence of dimple-like structures, where the fracture occurred. In Figure 10, a comparison of the SR1 and HIP+T6 fracture structures is represented.

The hardness test, while predictable for HIP+T6 for both orientations, with a decline in hardness as the aging hours increased, yielded an interesting outcome for SR1. The XY direction on SR1 exhibited little change during the aging, with an initial increase in hardness followed by a small decline, and a further decline within 1000 hours. The Z direction painted a different picture, showing an increase in hardness as the aging hours increased, peaking at 105 HV at 100 hours, the highest value among the SR1 values, yet falling short compared to HIP+T6. This high value of hardness was contrasted by the cycles the specimens endured, given that the Z direction on SR1 saw the least cycles survived compared to the XY orientation. Further research into the hardness values must be sought in order to classify this unique behavior. Further microstructure analysis, specifically the Si particles, could reveal why this occurs.

Overall, for applications within a stress range of 145 MPa and less than 100 hours aging, HIP+T6 is an ideal candidate, while for specimens treated with SR1, can work within a stress range of 124 MPa from 0 to 1000 aging hours, though thorough care should be applied through its manufacturing procedure.

References

- [1] J. Wu, X. Q. Wang, W. Wang, M. M. Attallah, and M. H. Loretto, "Microstructure and strength of selectively laser melted AlSi10Mg," *Acta Mater.*, vol. 117, pp. 311–320, Sep. 2016, doi: 10.1016/j.actamat.2016.07.012.
- [2] S. T. Nabil, E. Arrieta, R. B. Wicker, M. Benedict, and F. Medina, "EFFECT OF THERMAL AGING IN THE FATIGUE LIFE OF HOT ISOSTATIC PRESSED AlSi10Mg FABRICATED BY LASER POWDER BED FUSION".
- [3] R. F. Fernandes, J. Jesus, L. Borrego, J. M. Ferreira, and J. D. Costa, "Effect of heat treatment on fatigue crack growth performance of AlSi10Mg aluminum alloy submitted to LPBF," *Procedia Struct. Integr.*, vol. 42, pp. 1054–1060, 2022, doi: 10.1016/j.prostr.2022.12.133.
- [4] R. F. Fernandes, J. S. Jesus, L. Borrego, J. A. M. Ferreira, R. Branco, and J. D. M. Costa, "Effect of heat treatment on fatigue performance of notched and unnotched samples of AlSi10Mg manufactured by LPBF under variable loading amplitudes," *Procedia Struct. Integr.*, vol. 53, pp. 144–150, 2024, doi: 10.1016/j.prostr.2024.01.018.
- [5] Q. Yan, B. Song, and Y. Shi, "Comparative study of performance comparison of AlSi10Mg alloy prepared by selective laser melting and casting," *J. Mater. Sci. Technol.*, vol. 41, pp. 199–208, Mar. 2020, doi: 10.1016/j.jmst.2019.08.049.
- [6] Z. W. Xu, Q. Wang, X. S. Wang, C. H. Tan, M. H. Guo, and P. B. Gao, "High cycle fatigue performance of AlSi10mg alloy produced by selective laser melting," *Mech. Mater.*, vol. 148, p. 103499, Sep. 2020, doi: 10.1016/j.mechmat.2020.103499.
- [7] A. Sola and A. Nouri, "Microstructural porosity in additive manufacturing: The formation and detection of pores in metal parts fabricated by powder bed fusion," *J. Adv. Manuf. Process.*, vol. 1, no. 3, p. e10021, Jul. 2019, doi: 10.1002/amp2.10021.
- [8] O. Ertuğrul *et al.*, "Effect of HIP process and subsequent heat treatment on microstructure and mechanical properties of direct metal laser sintered AlSi10Mg alloy," *Rapid Prototyp. J.*, vol. 26, no. 8, pp. 1421–1434, Jun. 2020, doi: 10.1108/RPJ-07-2019-0180.
- [9] J. Merino *et al.*, "Multiple, comparative heat treatment and aging schedules for controlling the microstructures and mechanical properties of laser powder bed fusion fabricated AlSi10Mg alloy," *J. Mater. Res. Technol.*, vol. 13, pp. 669–685, Jul. 2021, doi: 10.1016/j.jmrt.2021.04.062.

- [10] A. Kumar Ramavajjala, T. R. Dandekar, R. K. Khatirkar, C. Joshi, R. N. Chouhan, and A. Agnihotri, "A review on the correlation between microstructure, heat treatment and mechanical properties of additively manufactured AlSi10Mg by LPBF," *Crit. Rev. Solid State Mater. Sci.*, vol. 50, no. 3, pp. 239–274, May 2025, doi: 10.1080/10408436.2024.2414012.
- [11] M. A. Balbaa, A. Ghasemi, E. Fereiduni, M. A. Elbestawi, S. D. Jadhav, and J.-P. Kruth, "Role of powder particle size on laser powder bed fusion processability of AlSi10mg alloy," *Addit. Manuf.*, vol. 37, p. 101630, Jan. 2021, doi: 10.1016/j.addma.2020.101630.
- [12] N. E. Uzan, R. Shneck, O. Yeheskel, and N. Frage, "Fatigue of AlSi10Mg specimens fabricated by additive manufacturing selective laser melting (AM-SLM)," *Mater. Sci. Eng. A*, vol. 704, pp. 229–237, Sep. 2017, doi: 10.1016/j.msea.2017.08.027.
- [13] F. Sajadi, J.-M. Tiemann, N. Bandari, A. Cheloe Darabi, J. Mola, and S. Schmauder, "Fatigue Improvement of AlSi10Mg Fabricated by Laser-Based Powder Bed Fusion through Heat Treatment," *Metals*, vol. 11, no. 5, p. 683, Apr. 2021, doi: 10.3390/met11050683.
- [14] "Technical Data EOS M290 ," EOS. <https://www.eos.info/metal-solutions/metal-printers/eos-m-290#technical-data> (accessed May 27, 2025)